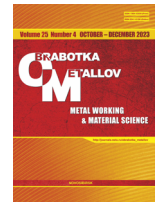




## Obrabotka metallov -

## Metal Working and Material Science

Journal homepage: [http://journals.nstu.ru/obrabotka\\_metallov](http://journals.nstu.ru/obrabotka_metallov)



### In situ crystal lattice analysis of nitride single-component and multilayer ZrN/CrN coatings in the process of thermal cycling

Andrey Vorontsov<sup>1, a</sup>, Andrey Filippov<sup>1, b, \*</sup>, Nikolay Shamarin<sup>1, c</sup>, Evgeny Moskvichev<sup>1, d</sup>,  
 Olga Novitskaya<sup>1, e</sup>, Evgeny Knyazhev<sup>1, f</sup>, Yulia Denisova<sup>2, g</sup>, Andrey Leonov<sup>2, h</sup>, Vladimir Denisov<sup>2, i</sup>

<sup>1</sup> Institute of Strength Physics and Materials Sciences SB RAS, 2/4 per. Academicheskii, Tomsk, 634055, Russian Federation

<sup>2</sup> Institute of High Current Electronics SB RAS, 2/3 per. Academicheskii, Tomsk, 634055, Russian Federation

<sup>a</sup>  <https://orcid.org/0000-0002-4334-7616>,  [vav@ispms.ru](mailto:vav@ispms.ru); <sup>b</sup>  <https://orcid.org/0000-0003-0487-8382>,  [andrey.v.filippov@yandex.ru](mailto:andrey.v.filippov@yandex.ru);  
<sup>c</sup>  <https://orcid.org/0000-0002-4649-6465>,  [shnn@ispms.ru](mailto:shnn@ispms.ru); <sup>d</sup>  <https://orcid.org/0000-0002-9139-0846>,  [em\\_tsu@mail.ru](mailto:em_tsu@mail.ru);  
<sup>e</sup>  <https://orcid.org/0000-0003-1043-4489>,  [nos@ispms.tsc.ru](mailto:nos@ispms.tsc.ru); <sup>f</sup>  <https://orcid.org/0000-0002-1984-9720>,  [zhenya4825@gmail.com](mailto:zhenya4825@gmail.com);  
<sup>g</sup>  <https://orcid.org/0000-0002-3069-1434>,  [yukolubaeva@mail.ru](mailto:yukolubaeva@mail.ru); <sup>h</sup>  <https://orcid.org/0000-0001-6645-3879>,  [laa-91@yandex.ru](mailto:laa-91@yandex.ru);  
<sup>i</sup>  <https://orcid.org/0000-0002-5446-2337>,  [volodyadenisov@yandex.ru](mailto:volodyadenisov@yandex.ru)

#### ARTICLE INFO

##### Article history:

Received: 20 September 2023

Revised: 26 September 2023

Accepted: 11 October 2023

Available online: 15 December 2023

##### Keywords:

Coating

Nitrides

Phase composition

RSA

CTE

Stresses

##### Funding

The work was carried out with the financial support of the Russian Federation represented by the Ministry of Science and Higher Education (project No. 075-15-2021-1348) within the framework of event No. 1.1.16.

##### Acknowledgements

Research were partially conducted at core facility “Structure, mechanical and physical properties of materials”.

#### ABSTRACT

**Introduction.** Thermal expansion is an important thermal and physical characteristic of materials, showing its expansion when heated. Knowing this property is important both from a scientific point of view and for practical applications. Materials with low thermal expansion are widely used in electronics, thermal barrier coatings and other applications. Mismatch in thermal expansion between different materials can lead to thermal stress on contact surfaces. The in-situ synchrotron X-ray diffraction method can detect this mismatch. Thermal stress requires an analysis of the coefficient of thermal expansion. Bulk expansion behavior is observed in thermally sprayed coatings. The CTE is important for designing and predicting coating performance under thermal stresses. Changes in the KTE can cause cracking and degradation of the coating. In-situ X-ray diffraction analysis helps to understand thermal expansion, crystallite size and stress and strain variation with temperature change. **The aim of this work** is to interpret and use in-situ high temperature X-ray diffraction as an effective tool to study the thermal mismatch behavior of a *W-Co* alloy substrate (8 % w/w *Co*, *WC* – matrix) with *CrN*, *ZrN* and *CrZrN* multilayer coatings and the characteristic differences between single component coatings and its combination in a multilayer coating. **Research Methodology.** In this work, specimens of chromium and zirconium nitride coatings deposited on *W-Co* hard alloy substrates were investigated. The fundamental method in this work is in-situ analysis using synchrotron radiation. The lattice parameter as a function of cycling temperature, the coefficient of thermal expansion during heating and cooling, and the thermal expansion mismatch between the substrate-coating pair and the coating layers in the multilayer coating were evaluated. **Results and discussion.** The lattice parameters and thermal expansion of the coatings are investigated. The lattice parameter of all coatings decreased during thermal cycling, indicating nitrogen evaporation. The multilayer coating has the least change in the parameter, possibly due to diffusion barriers. Lattice distortions do not differ between single and multilayer coatings. All coatings exhibit thermal expansion similar to the substrate. The multilayer coating creates conditions for compressive stresses in one phase and tensile stresses in the other phase, so the lifetime of multilayer coatings is expected to be high.

**For citation:** Vorontsov A.V., Filippov A.V., Shamarin N.N., Moskvichev E.N., Novitskaya O.S., Knyazhev E.O., Denisova Yu.A., Leonov A.A., Denisov V.V. In situ crystal lattice analysis of nitride single-component and multilayer ZrN/CrN coatings in the process of thermal cycling. *Obrabotka metallov (tehnologiya, oborudovanie, instrumenty) = Metal Working and Material Science*, 2023, vol. 25, no. 4, pp. 202–215. DOI: 10.17212/1994-6309-2023-25.4-202-215. (In Russian).

##### \* Corresponding author

Vorontsov Andrey V., Ph.D. (Engineering), Junior researcher  
 Institute of Strength Physics and Materials Sciences SB RAS,  
 2/4 per. Academicheskii,  
 634055, Tomsk, Russian Federation  
 Tel.: +7 (983) 239-34-17, e-mail: [vav@ispms.ru](mailto:vav@ispms.ru)

## Introduction

Thermal expansion is an important thermal and physical property of materials, indicating the degree of materials' extension upon heating. Knowledge of thermal expansion is of great interest not only from a scientific, but also from a practical point of view [1]. In assessing the potential uses of a material, thermal expansion becomes increasingly important in the production of parts and structures. Materials with low thermal expansion are widely used in electronic devices, thermal barrier coatings, precision equipment materials, thermal engine components, etc. [2]. In certain systems or composite materials, it is necessary to eliminate or even avoid thermal expansion mismatches between different materials, which can lead to the accumulation of thermal stress on the contact surfaces [3].

Thermal mismatch between the coating and substrate or between layers of a multilayer coating predominates during coating surfacing or heat treatment. Therefore, the resulting thermal stresses require a detailed analysis of the coefficient of thermal expansion (*CTE*) [4]. Oxide formation, residual stresses, and interfaces are characteristics of coatings caused by the thermal spraying process. Since volumetric expansion behavior is usually observed in thermally sprayed coatings, determining the correct *CTE* values is critical for designing and predicting coating characteristics under thermal loads [5]. Spray process parameters influence thermal expansion due to phase changes caused by oxidation, formation of compounds, etc. Thermal stresses arise from differences in *CTE* between the coating and substrate, and also arise as a result of the occurrence of a temperature gradient during the prolonged spraying process [6, 7]. It is also known that deformations due to thermal mismatch greatly affect the strength of component-coating bonding and the service life of thermal fatigue [8].

The coefficient of thermal expansion (*CTE*) quantitatively determines the expansion and contraction of a material due to temperature changes. The *CTE* of both the substrate and the coating strongly influences the adhesion strength of the coating. Significant changes in *CTE* can lead to deformation mismatch, causing cracks and degradation of the coating as a whole [9, 10]. The differences in thermal expansion coefficients at the interface result in a change in the local volume at the interface [11]. For example, in a coating on a *Ni*-based superalloy, the deformation mismatch between the coating and the substrate creates internal stresses in the coating, leading to damage to the coating interface layers [6].

In-situ X-ray diffraction analysis is a reliable tool for assessing temperature-dependent properties of substrates and coatings. It helps to understand thermal expansion, crystallite size, grain growth, and changes in stress and strain with temperature variations [12, 13]. Based on the literature cited, it can be stated that volumetric expansion and lattice distortion can induce internal stresses in the parent material. Therefore, to detect material mismatch processes in terms of thermophysical parameters, the use of in-situ synchrotron X-ray diffraction is appropriate [14]. The full-width at half-maximum (*FWHM*) of X-ray reflections can reflect the evolution of internal stress under thermal loading [15, 16]. For example, changes in interplanar spacing due to thermal expansion are associated with a specific crystallographic orientation, while peak broadening occurs when lattice defects are present in a sufficiently large amount within the scattering volume, as well as in the presence of micro-stresses.

As a result of thermal deformation mismatch, local residual stresses are generated, varying from grain to grain. The presence of grain-dependent lattice deformation along a crystallographic direction implies the existence of a distribution of interplanar distances (with a certain width  $\Delta d_{hkl}$ ) around a given "average" interplanar distance ( $d_{hkl}$ ) [17]. Sometimes, it is assumed that the intergranular stress state is constant and can, therefore, be ignored in the analysis. However, this assumption is often not valid [18]. The deformation of each grain depends on its orientation as well as the orientation of neighboring grains. If a grain is relatively "stiff" in a particular direction, the thermal stress in that direction induces plastic deformation in the "softer" surrounding grain. As a result, the deformation varies from grain to grain by an average magnitude, and the rate of stress decreases.

**The aim of this study** is to interpret and utilize in-situ high-temperature X-ray diffraction as an effective tool for investigating the behavior of thermal mismatch between the substrate of *VK8* alloy (92 % *WC*-8 % *Co*) and coatings of *CrN*, *ZrN*, and multilayer coating of *CrZrN*, as well as the characteristic

differences between single-component coatings and its combination in the multilayer coating. The evaluation of the crystal lattice parameter in the coatings and substrate, as well as its change during thermal cycling, was performed. The combination of the obtained data from in situ synchrotron studies made it possible to estimate the lattice distortions and thermal expansion parameters, which in turn enabled the evaluation of stress existence during thermal cycling. In-situ high-temperature X-ray diffraction may potentially serve as a fast method for studying thermal mismatch caused by the thermal expansion of the substrate and coating, as well as a method for further optimization of the obtained coatings with minimal differences in the physical properties of the coating materials.

## Methods and materials

In-situ synchrotron X-ray diffraction measurements at high X-ray energies were performed during cooling and heating on the *VEPP-3* beamline at Novosibirsk, Russia. The X-ray beam had a size of  $1 \times 2$  mm, a wavelength of 0.1 nm, and a photon energy of 12.4 keV. The specimens were initially heated from 30 °C to 550 °C and then cooled to 30 °C at a rate of 60 °C/min; in total, 3 heating-cooling cycles were performed. X-ray diffraction patterns were recorded at intervals of 30 °C. The interplanar distance ( $d$ ) and the full-width at half-maximum ( $FWHM$ ) of the diffraction peaks were obtained by fitting the diffraction reflections with a *Gaussian* distribution function. The lattice thermal expansion is determined by the change in strain of the  $d$ -space with temperature variation. The first derivative of the lattice thermal expansion curve, divided by the initial interplanar distance of the corresponding reflection plane, is defined as the lattice thermal expansion coefficient. The peak width includes instrumental broadening, specimen size variation, grain size broadening, and micro-stresses [15, 16]. In this experiment, instrumental broadening and grain size broadening are assumed to remain constant with temperature variation, so any changes in  $FWHM$  are attributed to the evolution of stresses.

## Results and discussion

Fig. 1 shows the dynamic changes in the lattice parameter during thermal cycling. Here and throughout, the left part of the figure refers to homogeneous coatings and substrates with single-component coatings (suffix “mono”), while the right part of the figure represents the components of the multilayer coating and substrate with the applied multilayer coating (suffix “*CrZrN* 8 rpm”). The start of the thermal cycling process is indicated by a *diamond*, and the end of the process is denoted by a *star*. In all cases depicted in fig. 1, an increase in the lattice parameter (calculated from the (111) reflection) is observed during heating, followed by a decrease during cooling. However, it is found that the lattice parameter changes globally when comparing its value at the beginning and after the testing. This is demonstrated by the fitted straight line that extends throughout the testing period. The slope of this line indicates the extent of the lattice parameter change.

When comparing the lattice parameter of the same phase for the *ZrN* mono specimen (Fig. 1a) and the *CrZrN* 8 rpm specimen (fig. 1b), the differences in the change of the lattice parameter are insignificant and follow a similar trend, even though the actual value of the lattice parameter in the *ZrN* component of the multilayer coating initially differed significantly and was smaller by 0.03 Å. When comparing the *CrN* phase in the *CrN* mono specimens and the *CrZrN* 8 rpm specimens, the rate of change (slope of the straight line) of the lattice parameter differs by an order of magnitude. This suggests that in the *CrN* mono specimen (fig. 1c), nitrogen depletion occurs to a greater extent during thermal cycling compared to the multilayer coating (fig. 1d) despite the initial difference in the lattice parameter of 0.125 Å. The lattice parameter, calculated from the (101) reflection, as well as its changes for the polycrystalline substrate, does not differ significantly, but will be considered later.

The constructed hysteresis loops of the lattice parameter versus temperature during thermal cycling (fig. 2) provide insights not only into the differences in the magnitude of the lattice parameter but also reveal that the largest change (reduction) in the lattice parameter for all coatings occurs after the first

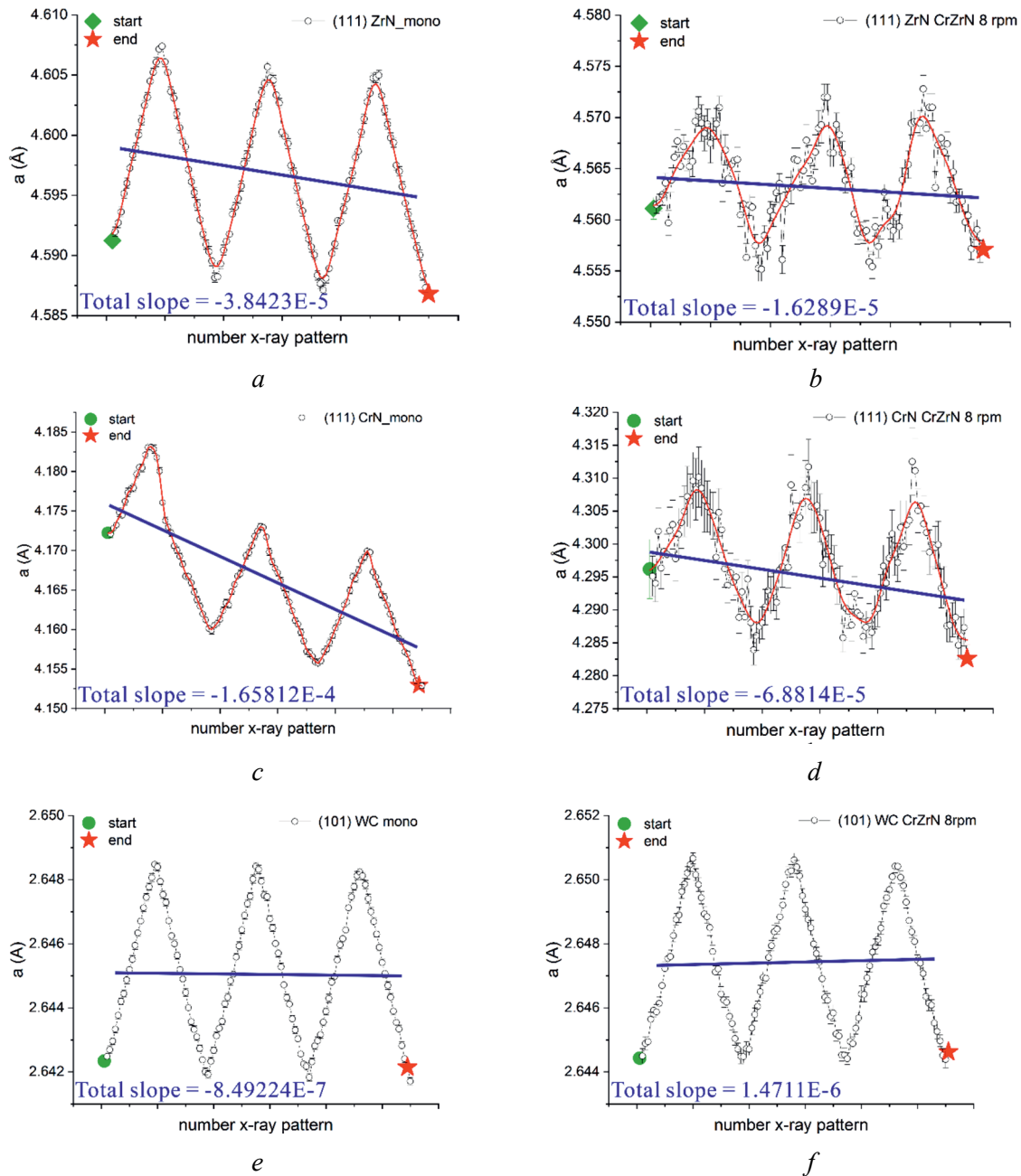


Fig. 1. Dynamic pattern of the lattice parameter of the components of single-component coatings (*a*, *c*), multilayer coatings (*b*, *d*) and substrate (*e*, *f*) as a function of time (X-ray diffraction numbers). The straight line and the value of the slope of this straight line indicate the general change of the lattice parameter during thermal cycling

heating cycle, as particularly evident in fig. 2, *c* (*CrN* mono specimen). However, the relationship between the lattice parameter and temperature within the cycle for the *ZrN* component of the multilayer coating (fig. 2, *b*) remains unclear. The intersecting fitted curves within the cycle in this case can be attributed to thermal stresses. Similar dependencies for the substrate material, the *WC* phase, were not observed, as the lattice parameter changes within the error range during the thermal cycling process. For the substrate, which has a hexagonal symmetry, only the reflection from the (101) plane is investigated for the same reason.

The coefficient of thermal expansion (*CTE*) during thermal cycling is shown in fig. 3. Based on the logic of the thermal cycling process and the existence of extrema in the dependence, the graph in fig. 3 is presented as the absolute value of the ordinate axis. The single-component specimens presented in figs. 3, *a*, *c*, *d* demonstrate a cyclic *CTE* with good repeatability within the temperature range from 100 °C to 450 °C. For the *ZrN* mono and *CrN* mono coating materials, the average *CTE* is  $18 \times 10^{-6} \text{ } ^\circ\text{C}^{-1}$ . In contrast, for the

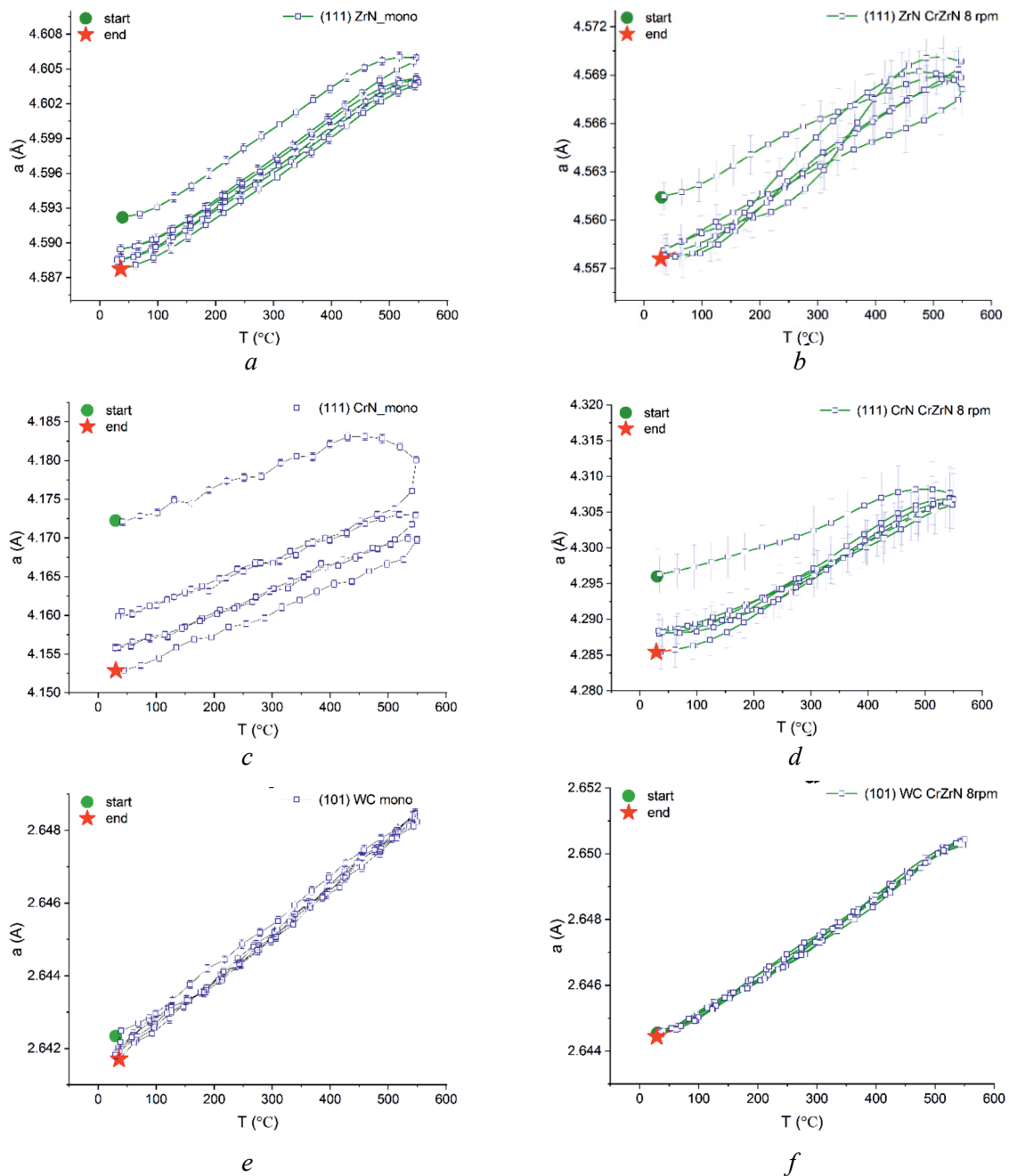


Fig. 2. Dynamics of changes in the lattice parameter of the components of single-component coatings (*a, c*), multilayer coatings (*b, d*) and substrate (*e, f*) as a function of temperature during thermal cycling

substrate material (*WC*), the *CTE* in the specified temperature range is  $43.5 \times 10^{-6} \text{ }^\circ\text{C}^{-1}$ , which is 2.4 times higher than the *CTE* for the coating material. Deviations from a linear *CTE* are observed at temperatures below  $100 \text{ }^\circ\text{C}$  and above  $450 \text{ }^\circ\text{C}$ . This is particularly evident during the first heating of the *ZrN* mono and *CrN* mono coatings, indicated by red dots in figs. 3a and 3c. Additionally, the *CTE* behavior of the *CrN* mono coating shows a consistent decrease within the temperature range from  $550 \text{ }^\circ\text{C}$  to  $500 \text{ }^\circ\text{C}$  during cooling.

When calculating the *CTE* for the multilayer coatings, it is found that linear sections of the *CTE* are almost absent. The *CTE* for the components of the multilayer coating and substrate is presented in figs. 3, *b, d, e*. Based on this data, it can be concluded that the multilayer coating led to an increase in the *CTE* magnitude, and the *CTE* of the substrate material also increased (figs. 3, *b, d, e*) compared to the single-component coatings. In this case, the lowest *CTE* value is found for the *ZrN* phase, which is  $26.3 \times 10^{-6} \text{ }^\circ\text{C}^{-1}$  during heating and an average of  $43.7 \times 10^{-6} \text{ }^\circ\text{C}^{-1}$  during cooling. The *CTE* values for the *CrN* component

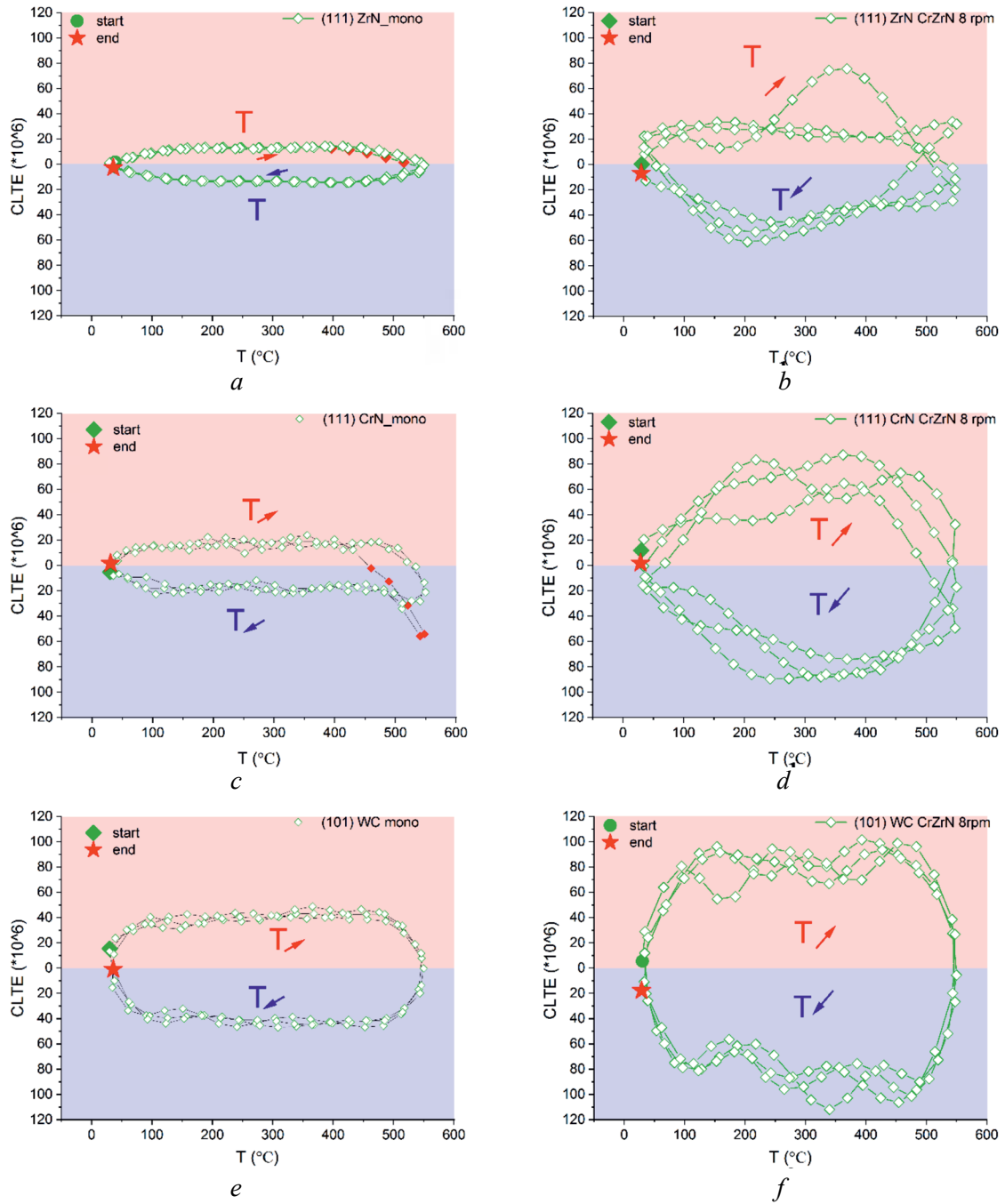


Fig. 3. Thermal expansion coefficient during thermal cycling of components of single-component coatings (a, c), multilayer coatings (b, d) and substrate (e, f)

of the multilayer coating are in the range of  $60$  to  $80 \times 10^{-6} \text{ }^\circ\text{C}^{-1}$ , while the *CTE* of the *WC* substrate phase is determined to be an average of  $80 \times 10^{-6} \text{ }^\circ\text{C}^{-1}$ . Overall, there is a general increase in *CTE* for the multilayer coatings (figs. 3, b, d, e) compared to the *CTE* of the single-component coatings.

The deformation presented here represents uniaxial strain calculated using equation

$$\varepsilon = \frac{d_{hkl}(T) - d_{in}}{d_{in}},$$

where  $d_{hkl}(T)$  is the interplanar distance measured at temperature  $T$  in the specimen for the diffraction reflection created by the lattice plane (hkl), and  $d_{in}$  represents the reference interplanar distance for that diffraction reflection.

Figs. 4, *a–d* demonstrate the deformation change of the lattice for the investigated nitride coatings throughout the entire thermal cycling process, while the lattice deformation of the *VK8* alloy substrate coating shows periodic behavior and linear dependence.

Interestingly, the lattice deformation gradually increases with temperature up to 800 °C, which is usually uncommon. Stressed lattices typically relax at high temperatures.

Fig. 5 illustrates the evolution of the *FWHM* (full-width at half-maximum) of selected reflection planes for the nitride coatings and substrate. It is evident that the *FWHM* dependencies of the crystalline planes differ between the specimens with single-component coatings (figs. 5, *a, c, d*) and the specimens with multilayer coatings (figs. 5, *b, e*).

Distinguishing between heating and cooling cycles based on the *FWHM* data proved to be impossible for the *CrN* phase of both the single-component (fig. 5, *c*) and multilayer (fig. 5, *d*) coatings. In these cases,

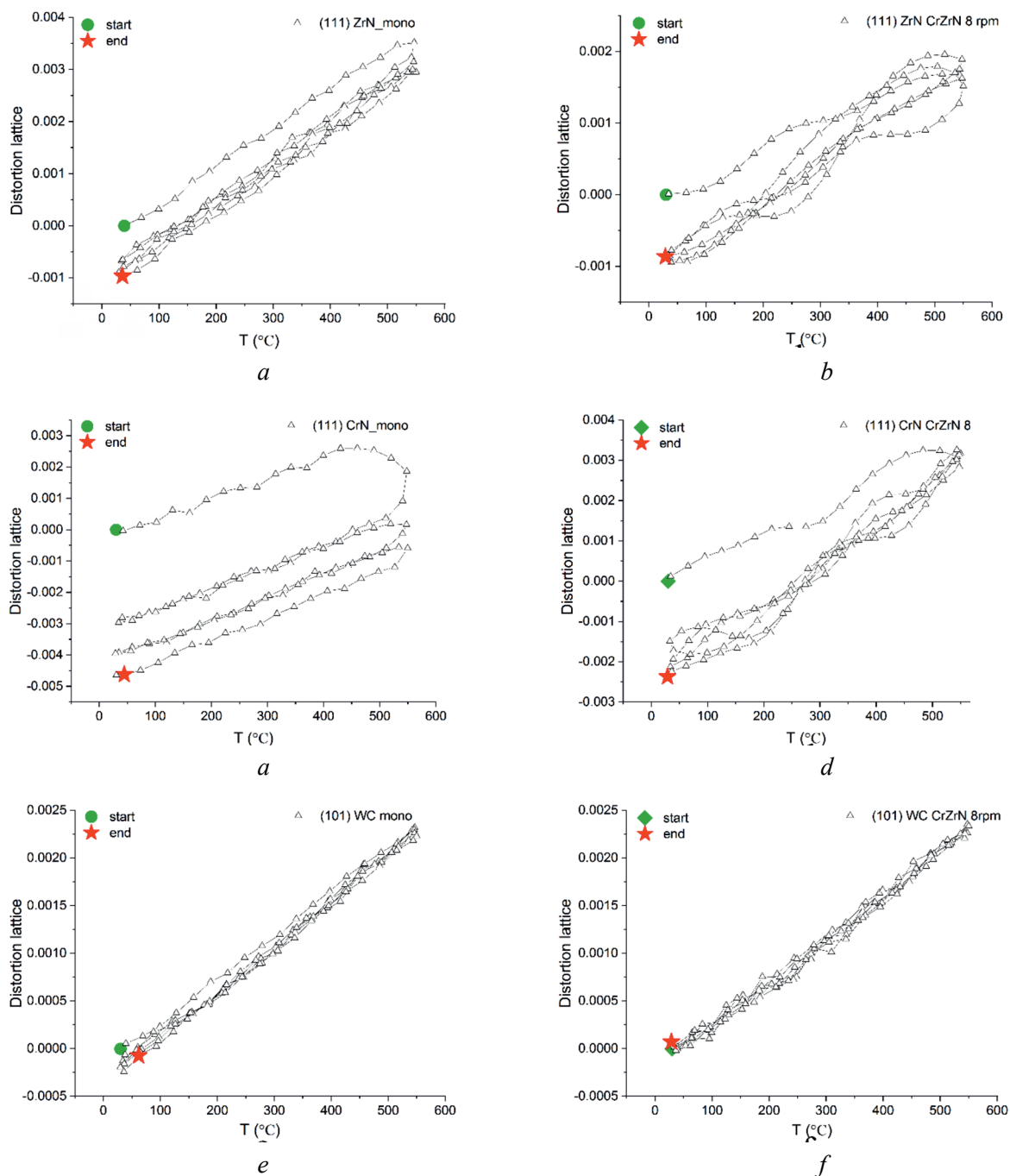


Fig. 4. Crystal lattice deformations as a function of temperature of the thermal cycling process of components of single-component coatings (*a, c*), multilayer coatings (*b, d*) and substrate (*e, f*)

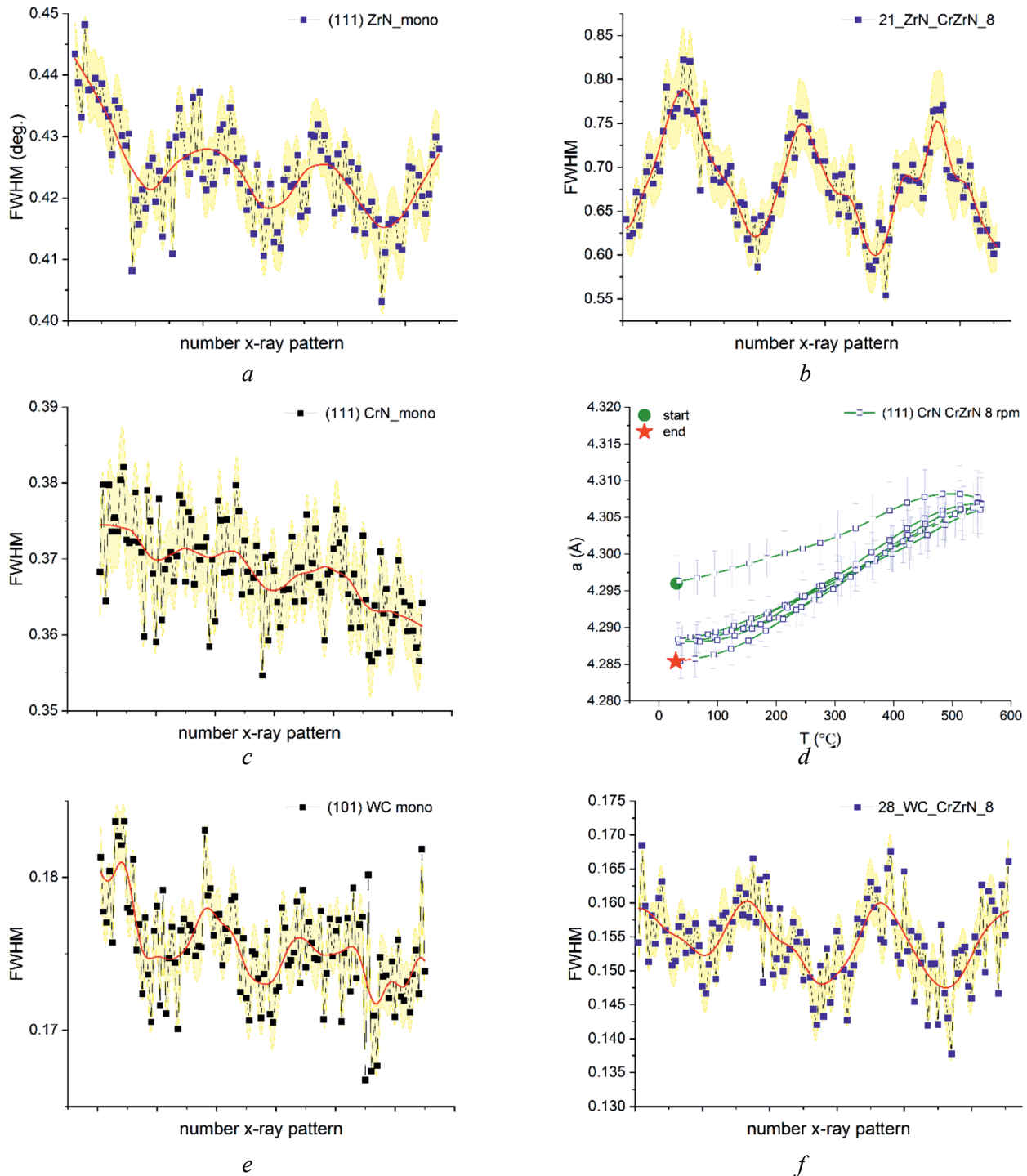


Fig. 5. *FWHM* evolution of selected reflection planes of nitride single-component coatings (a, c), multilayer coatings (b, d) and substrate (e, f)

a general slope of the *FWHM* dependence with respect to the thermal cycling time is observed. In the case of the *ZrN* phase of the single-component (fig. 5, a) and multilayer (fig. 5, b) coatings, periodic increases and decreases in *FWHM* values are observed. Moreover, compared to the similar graph for the substrate, the periods of *FWHM* variation occur with a shift of half a period for the specimen with the multilayer coating (figs. 5, b, e). Conversely, for the specimen with the single-component coating (figs. 5, a, d), the periods of *FWHM* decrease and increase coincide.

It should be noted that the *FWHM* (full-width at half-maximum) of the (111) plane for the nitride coatings generally remains almost unchanged before and after the thermal cycling process. The trend of

the *FWHM* variation, where the peaks' maxima and minima coincide at different temperatures, can be attributed to the occurrence of a low lattice thermal expansion coefficient in all directions of the specimen.

Through the analysis of in-situ data presented above, we can understand the correlation between thermal expansion and internal stress. The *FWHM* of X-ray diffraction peaks is often used to measure internal stress caused by lattice defects [19]. In this study, the gradual increase in *FWHM* demonstrates the gradual increase in lattice distortions caused by interfaces between the substrate and coatings, as well as between individual layers of the multilayer coatings.

As shown in figs. 3 and 5, the increase in *FWHM* coincided with a decrease in the thermal expansion coefficient, indicating that the accumulation of internal stress leads to volumetric expansion, which compensates for some of the lattice shrinkage of the original phase during cooling.

It is worth noting that the *FWHM* values for the single-component coatings and its substrate decreased with increasing temperature (figs. 5, *a*, *c*, *d*). The reduction in peak broadening indicates the relaxation of residual stresses [13]. On the other hand, the *FWHM* increased with increasing temperature for the *ZrN* phase in the multilayer coating (fig. 5, *b*). Some studies attribute this effect to the presence of residual stresses coupled with an induced phase transformation [20]. Alternatively, under our thermal cycling conditions, the *ZrN* phase in the multilayer coating may experience compression from the second component of the multilayer coating, *CrN*, thereby inducing a stressed state. Additionally, nitrogen evaporation, which leads to changes in the chemical composition of the coating, can also affect the lattice parameter and create internal stresses [21].

The overall residual stress in the components includes internal stress, thermal stress, and external stress. During thermal processing, the change in each component of residual stress affects both the substrate and the coating layers due to differences in thermal expansion coefficients (*CTE*) and is attributed to the variation of thermal stress with temperature. Since the *CTE* of the *ZrN* and *CrN* phases in the single-component coatings was lower than that of the *VK8* alloy substrate (figs. 3, *a*, *c*, *d*), an increase in tensile stress is observed in the *ZrN* and *CrN* layers upon heating [22]. However, the situation changes when analyzing the *CTE* of the present phases in the multilayer coating. As shown in figs. 3b, 3d, and 3e, the substrate and the *CrN* phase exhibit the highest *CTE* values ( $60\text{--}80 \times 10^{-6} \text{ C}^{-1}$ ), while the *ZrN* phase has the lowest *CTE*, with values of  $30 \times 10^{-6} \text{ C}^{-1}$  during heating and  $40 \times 10^{-6} \text{ C}^{-1}$  during cooling. Therefore, between the *ZrN*, *CrN*, and *WC* phases in the multilayer coating, conditions are created during heating that induce compressive stress in the *CrN* phase and tensile stress in the *ZrN* phase [23].

## Conclusions

This study investigated the behavior of thermal expansion and lattice parameter changes in relation to the development of internal stresses during thermal cycling. Based on the experimental data, the following conclusions can be drawn:

1. The lattice parameter of all coatings decreased during thermal cycling, indicating nitrogen evaporation and changes in the chemical composition of the coatings under thermal load. The multilayer coating showed the least variation in the lattice parameter, indicating the presence of diffusion barriers for nitrogen.
2. The analysis of the crystal lattice distortions of the coating components of the studied specimens did not reveal significant differences between single-component and multilayer coatings;
3. All studied coatings displayed thermal expansion comparable to that of the substrate. The slightly higher thermal expansion of the substrate in the single-component coatings resulted in tensile stresses at the interface. Between the *ZrN* and *CrN* phases of the multilayer coating and the *WC* phase of the substrate, conditions were created during heating that induced compressive stresses in the *CrN* phase and tensile stresses in the *ZrN* phase. As a result, it can be expected that the service life of multilayer coatings will be higher compared to single-component coatings.

## References

1. Krishnan R.S., Srinivasan R., Devanarayanan S. Theory of thermal expansion of crystals. *Thermal expansion of crystals*. Pergamon Press, 1979, ch. 3, pp. 54–104. DOI: 10.1016/B978-0-08-021405-4.50008-1.
2. Roy R., Agrawal D.K., McKinstry H.A. Very low thermal expansion coefficient materials. *Annual Review of Material Science*, 1989, vol. 19, pp. 59–81. DOI: 10.1146/annurev.ms.19.080189.000423.
3. Padture N.P., Gell M., Jordan E.H. Thermal barrier coatings for gas-turbine engine applications. *Science*, 2002, vol. 296, pp. 280–284. DOI: 10.1126/science.1068609.
4. Wang C., Yang J., Huang W., Zhang T., Yan D., Pu J., Chi B., Li J. Numerical simulation and analysis of thermal stress distributions for a planar solid oxide fuel cell stack with external manifold structure. *International Journal of Hydrogen Energy*, 2018, vol. 43, pp. 20900–20910. DOI: 10.1016/j.ijhydene.2018.08.076.
5. Bejarano M.L., Valarezo A., Lara-Curzio E., Sampath S. Dilation behavior of thermal spray coatings. *Journal of Thermal Spray Technology*, 2019, vol. 28, pp. 1851–1866. DOI: 10.1007/s11666-019-00927-4.
6. Tao S., Yang J., Shao F., Zhao H., Zhong X., Zhuang Y., Sheng J., Ni J., Li Q., Tao S. Atmospheric plasma sprayed thick thermal barrier coatings: Microstructure, thermal shock behaviors and failure mechanism. *Engineering Failure Analysis*, 2022, vol. 131. DOI: 10.1016/j.engfailanal.2021.105819.
7. Kustov S., Golyandin S., Sapozhnikov K., Vincent A., Maire E., Lormand G. Structural and transient internal friction due to thermal expansion mismatch between matrix and reinforcement in Al-SiC particulate composite. *Materials Science and Engineering: A*, 2001, vol. 313, pp. 218–226. DOI: 10.1016/S0921-5093(01)00971-6.
8. Khor K.A., Dong Z.L., Gu Y.W. Plasma sprayed functionally graded thermal barrier coatings. *Materials Letters*, 1999, vol. 38, pp. 437–444. DOI: 10.1016/S0167-577X(98)00203-1.
9. Öztürk B., Topcu A., Cora Ö.N. Influence of processing parameters on the porosity, thermal expansion, and oxidation behavior of consolidated Fe22Cr stainless steel powder. *Powder Technology*, 2021, vol. 382, pp. 199–207. DOI: 10.1016/j.powtec.2020.12.072.
10. Loghman-Estarki M.R., Shoja Razavi R., Edris H., Pourbafrany M., Jamali H., Ghasemi R. Life time of new SYSZ thermal barrier coatings produced by plasma spraying method under thermal shock test and high temperature treatment. *Ceramics International*, 2014, vol. 40, pp. 1405–1414. DOI: 10.1016/j.ceramint.2013.07.023.
11. Khan M.A., Anand A.V., Duraiselvam M., Rao K.S., Singh R.A., Jayalakshmi S. Thermal shock resistance and thermal insulation capability of laser-glazed functionally graded lanthanum magnesium hexaluminate/yttria-stabilised zirconia thermal barrier coating. *Materials (Basel)*, 2021, vol. 14. DOI: 10.3390/ma14143865.
12. Purushotham N., Parthasarathi N.L., Babu P.S., Sivakumar G., Rajasekaran B. Effect of thermal expansion on the high temperature wear resistance of Ni-20%Cr detonation spray coating on IN718 substrate. *Surface and Coatings Technology*, 2023, vol. 462. DOI: 10.1016/j.surfcoat.2023.129490.
13. Kaschel F.R., Vijayaraghavan R.K., Shmeliov A., McCarthy E.K., Canavan M., McNally P.J., Dowling D.P., Nicolosi V., Celikin M. Mechanism of stress relaxation and phase transformation in additively manufactured Ti-6Al-4V via in situ high temperature XRD and TEM analyses. *Acta Materialia*, 2020, vol. 188, pp. 720–732. DOI: 10.1016/j.actamat.2020.02.056.
14. Meng Q.-K., Xu J.-D., Li H., Zhao C.-H., Qi J.-Q., Wei F.-X., Sui Y.-W., Ma W. Phase transformations and mechanical properties of a Ti<sub>36</sub>Nb<sub>5</sub>Zr alloy subjected to thermomechanical treatments. *Rare Metals*, 2022, vol. 41, pp. 209–217. DOI: 10.1007/s12598-021-01744-x.
15. Shiman O.V., Skippon T., Tulk E., Daymond M.R. Strain evolution in Zr-2.5 wt% Nb observed with synchrotron X-ray diffraction. *Materials Characterization*, 2018, vol. 146, pp. 35–46. DOI: 10.1016/j.matchar.2018.09.022.
16. Qian L.H., Wang S.C., Zhao Y.H., Lu K. Microstrain effect on thermal properties of nanocrystalline Cu. *Acta Materialia*, 2002, vol. 50, pp. 3425–3434. DOI: 10.1016/S1359-6454(02)00155-6.
17. Daymond M.R. Internal stresses in deformed crystalline aggregates. *Reviews in Mineralogy and Geochemistry*, 2006, vol. 63, pp. 427–458. DOI: 10.2138/rmg.2006.63.16.
18. Repper J., Hofmann M., Krempaszky C., Regener B., Berhuber E., Petry W., Werner E. Effect of macroscopic relaxation on residual stress analysis by diffraction methods. *Journal of Applied Physics*, 2012, vol. 112, p. 64906. DOI: 10.1063/1.4752877.
19. Fujita F.E. A statistical thermodynamic theory of pre-martensitic tweed structure. *Materials Science and Engineering: A*, 1990, vol. 127, pp. 243–248. DOI: 10.1016/0921-5093(90)90315-T.
20. Londoño-Restrepo S.M., Herrera-Lara M., Bernal-Alvarez L.R., Rivera-Muñoz E.M., Rodríguez-García M.E. In situ XRD study of the crystal size transition of hydroxyapatite from swine bone. *Ceramics International*, 2020, vol. 46, pp. 24454–24461. DOI: 10.1016/j.ceramint.2020.06.230.



21. Youssef L., Kinfack Leoga A.J., Roualdes S., Bassil J., Zakhour M., Rouessac V., Ayrat A., Nakhil M. Optimization of N-doped TiO<sub>2</sub> multifunctional thin layers by low frequency PECVD process. *Journal of the European Ceramic Society*, 2017, vol. 37, pp. 5289–5303. DOI: 10.1016/j.jeurceramsoc.2017.05.010.

22. Daniel R., Holec D., Bartosik M., Keckes J., Mitterer C. Size effect of thermal expansion and thermal/intrinsic stresses in nanostructured thin films: Experiment and model. *Acta Materialia*, 2011, vol. 59, pp. 6631–6645. DOI: 10.1016/j.actamat.2011.07.018.

23. Manjunath N., Santhy K., Rajasekaran B. The effect of strain induced phase transformation on the thermal expansion compatibility of plasma sprayed spinel coating on SOFC metallic interconnect – A study using in situ high temperature X-ray diffraction. *International Journal of Hydrogen Energy*, 2023, vol. 48 (81), pp. 31767–31768. DOI: 10.1016/j.ijhydene.2023.04.322.

## Conflicts of Interest

The authors declare no conflict of interest.

© 2023 The Authors. Published by Novosibirsk State Technical University. This is an open access article under the CC BY license (<http://creativecommons.org/licenses/by/4.0>).

